RSC Advances

PAPER

View Article Online
View Journal | View Issue

CrossMark click for updates

Cite this: *RSC Adv.*, 2017, **7**, 15116

Evaluation of hydrodeoxygenation reactivity of pyrolysis bio-oil with various Ni-based catalysts for improvement of fuel properties

Shinyoung Oh,[a] Hang Seok Choi,[b] In-Gyu Choi[a] and Joon Weon Choi*[c]

Three Ni-based catalysts were prepared for hydrodeoxygenation (HDO) of bio-oil with three different support materials (active carbon, SBA-15 and Al-SBA-15) and their catalytic effects were tested with crude bio-oil at 300 °C and under 3 MPa H_2 pressure for 60 min. After the HDO reaction, gas, liquid phase (light oil and heavy oil) and char were obtained as the primary products. Heavy oil was produced at a yield of 45.8–48.1 wt%, with no significant differences among the three catalysts. Mesoporous silica-supported catalysts (Ni/SBA-15 and Ni/Al-SBA-15) produced large amounts of char (16.3–18.6%), while Ni/C yielded 8.5 wt% char. Active carbon-supported catalysts (Ni/C) yielded more gas (27.7%) than the Ni/SBA-15 and Ni/Al-SBA-15 catalysts (6.6–8.9%), due to high surface area and low char deposition on the active carbon-supported catalysts. The HDO reaction led to improvement in the fuel properties of crude bio-oil. The water content, acidity, viscosity and oxygen content decreased *via* de-moisturization, *i.e.*, dehydration, as well as dehydroxylation, resulting in an increase in heating value. The heavy oil obtained from HDO with Ni/Al-SBA-15 exhibited a low water content (9.3 wt%), while that of Ni/SBA-15 revealed a high HHV (22.8 MJ kg^{-1}), energy efficiency (62.8%), and degree of deoxygenation (54.9%). A major factor of bio/oil instability is unstable oxygen-containing compounds, such as acetic acid, furfural, vanillin and levoglucosan, which were obviously reduced in the heavy oil in this study.

Received 26th January 2017
Accepted 1st March 2017

DOI: 10.1039/c7ra01166k

rsc.li/rsc-advances

Open Access Article. Published on 07 March 2017. Downloaded on 1/14/2026 8:37:09 PM.
This article is licensed under a Creative Commons Attribution 3.0 Unported Licence.

1. Introduction

Improvements in bio-oil quality and stability can be achieved by the upgrading process hydrodeoxygenation, an interesting alternative to well-enhanced biofuel production. This process occurs simultaneously with hydrodesulphurization, hydrodenitrogenation, and hydrodemetallization, and removes the oxygens of oxygenated compounds and converts them to esters or ketones *via* hydrogenolysis, hydrogenation, dealkylation, dehydration, decarbonylation, or dehydroxylation. Furthermore, depolymerization, transalkylation, hydrogenation, and further cracking of compounds in bio-oil can also be significant depending on the characteristics of the catalysts, and these reactions can contribute to improve the bio-oil quality.[1,2] Hydrodeoyxgenation (HDO) is attracting a great deal of attention because it can enhance the bio-oil quality to overcome disadvantages such as high water content, acidity, viscosity, oxygen level, and low heating value under high pressure.[3,4] Some of previous studies conducted HDO with lignin model compounds. Guaiacol converted into *o*-cresol, phenol or benzene.[5] Anisole and catechol also converted into phenol, benzene or cyclohexane *via* hydrodeoxygenation.[6,7] Generally, most of phenolic compounds were methylated, hydrogenated, demethoxylated of dehydroxylated during the HDO process. Coumaran alkyl ether bond and b-*O*-4 bond in dimeric lignin model compounds were cleaved during HDO, while 5–5 linkages were not.[7]

General HDO catalysts, which are based on sulfided CoMo, NiMo or noble metal catalysts, show good performance in the enhancement of bio-oil. However, the need for a supply of sulfur-containing compounds and potential of sulfur contamination in bio-oil represent significant difficulties. Noble metals, generally dispersed on zeolites such as ZSM-5 or active charcoal supports, are efficiently applied to the HDO of bio-oil. However, the noble metal phase is expensive, and its utilization affects the economy of the HDO reaction.[8,9]

Supported non-noble metal catalysts, such as Fe/SiO_2, Co/SiO_2, and Ni-based materials, have been recently used in HDO studies. Transition metal catalysts, especially Ni or Cu, were promoted hydrogenation, decarboxylation and decarbonylation.[10] Moreover, its electronic properties can perform similar reactions as Pd or Pt such as cleavage C–C or C–H for hydrocarbon or alcohol reforming.[11] Although Ni-based catalysts show greater activity than other catalysts, coke deposition

[a]*Department of Forest Sciences, Seoul National University, 599 Gwanak-ro, Gwanak-gu, Seoul, 151-921, Korea*

[b]*Department of Environmental Engineering, Yonsei University, Wonju 220-710, Korea*

[c]*Graduate School of International Agricultural Technology, Institute of Green-Bio Science and Technology, Seoul National University, Pyeongchang 232-916, Gangwon-do, Korea. E-mail: cjw@snu.ac.kr; Fax: +82-33-339-5830; Tel: +82-33-339-5840*

This journal is © The Royal Society of Chemistry 2017

Open Access Article. Published on 07 March 2017. Downloaded on 1/14/2026 8:37:09 PM.
This article is licensed under a Creative Commons Attribution 3.0 Unported Licence.

is still a problem for bio-oil upgrading.[12] According to Wang,[13] RANEY® nickel and other nickel catalysts can catalyze the transfer hydrogenation of ketones, phenols, aldehydes, olefins, and aromatic alcohols with 2-PrOH as an H-donor. Zhang *et al.* investigated that Ni could cleave the C–O bonds in lignin under severe condition. Especially Ni/C catalyzed lignin hydrogenolysis under mild condition with polar solvent.[14]

Mesoporous silica materials have noted as catalyst supports due to their high specific surface areas, narrow range of pore size distributions, and large pore volumes. Therefore, mesoporous silica supports are desirable alternative silica supports based on their control of catalyst particle size and influence in product selectivity through transport effects.[15] Alumina is occasionally added to produce structures with silica mesoporous supports in order to assign acidic sites that can act as active sites. To create catalytic active sites for mesoporous silica supports, the supports are doped with metal. Among the mesoporous silicate supports (M41S, SBA, MSU, HMS, *etc.*), SBA-15 has the largest pore, with hexagonally regio-regular arranged mesopores, adjustable pore size, and high thermal stability.[4,16,17] Moreover, SBA-15 was found to be significantly more effective in deoxygenation than the HMS-supported catalyst.[18] Supporting these active phases in meso-structured supports might contribute to complete utilization of their catalytic properties by promoting dispersion and increasing the number of active sites.

Therefore, in the present work, Ni particles were distributed uniformly inside active charcoal and meso-structured supports (SBA-15 and Al-SBA-15) to investigate the effect of Ni based catalysts on the HDO reaction of bio-oil.

2. Experimental

2.1. Synthesis of SBA-15 and Al-SBA-15 supports by a sol–gel method

Mesoporous SBA-15 or Al-SBA-15 was synthesized by sol–gel method,[19] using poly(ethylene glycol)-*block*-poly(propylene glycol)-*block*-poly(ethylene glycol) (Pluronic P123, average $M_n \sim 5{,}800$, Aldrich) as the structure-directing agent, tetraethyl orthosilicate (TEOS, Aldrich) as the silicate source, and aluminium isopropoxide (AIP, Aldrich) in order to obtain the desired Si/Al ratio and acid sites on the supports under acidic conditions. All commercial chemicals were used without further purifications. SBA-15 and Al-SBA-15 were obtained as follows:

8 g of Pluronic 123 was dissolved in 250 mL of 1.9 M HCl, heated to 40 °C, and TEOS was added. After stirring for 20 h at 40 °C, the mixture was aged at 110 °C for 24 h. For Al-SBA-15, 8.5 g of TEOS and 0.125 g of AIP were added to 10 mL of 1.9 M HCl. After stirring for 3 h, the homogenous mixture was added to a solution of 4 g of Pluronic 123 dissolved in 150 mL of 1.9 M HCl. The solution was stirred for 20 h at 40 °C and then aged at 110 °C for 24 h. The solid product was recovered by filtration, dried overnight and calcined at 550 °C for 5 h under static air.

2.2. Preparation of the Ni-based catalyst by the wet impregnation method

Synthesized SBA-15, Al-SBA-15, and commercial activated charcoal (~100 mesh particle size, Sigma-Aldrich) were used as Ni-based catalyst supports. The catalytic active site, nickel, was loaded on SBA-15, Al-SBA-15, or activated charcoal support by a wet impregnation method,[19,20] as follows.

An equal amount of $Ni(NO_3)_2 \cdot 6H_2O$ solution and supports (active charcoal, SBA-15, and Al-SBA-15) were stirred for 1 h. The mixture was then dried at 80 °C and calcined in air at 550 °C for 3 h to obtain Ni/C, Ni/SBA-15, and Ni/Al-SBA-15. The catalysts were reduced at 800 °C for 3 h under an H_2 atmosphere before use.

2.3. Catalyst characterization

The morphology of each of the three catalysts (Ni/C, Ni/SBA-15, and Ni/Al-SBA-15) was investigated by FE-SEM and SEM-EDS (field-emission scanning electron microscopy, SIGMA). The specific surface areas of the support and catalysts were measured by the Brunauer–Emmett–Teller (BET) test, and the pore distribution and cumulative volumes of the pores were obtained by the Barrett–Joyner–Halenda (BJH) method from the desorption branches of the N_2 isotherms measured at 77.3 K. Samples were degassed at 373 K for 4 h before the tests. The acidity of the catalysts was measured by the NH_3-TPD (BELCAT II). Before the adsorption, the 0.05 g of the catalyst was dried in a 50 mL min^{-1} of predried (500 °C) He for 110 min. Then adsorption took place with 5% NH_3 in He at 100 °C for 30 min. X-ray powder diffraction patterns (XRD) were analyzed by a Bruker D8 Advance with DAVINCI using Cu Kα radiation (λ = 1.5418 Å), operated at 40 kV and 40 mA with a scan speed of 0.5 s min^{-1} in a range of 10–70 degrees (2 theta). The Si/Al ratio of Al-SBA-15 and the metal content of the catalysts were measured by inductively coupled plasma optical emission spectroscopy (ICP-ES, Multiwave PRO, Anton Parr). The samples were digested in acids (HF, HNO_3, H_2O_2) for ICP-ES analysis. The surface properties of the catalysts were analyzed by AXIS-HIS (Kractos Inc.). X-ray photoelectron spectroscopy (XPS) was performed using Mg in a Mg/Al dual anode (15 mA, 12 kV), and the spectra were analyzed using Casa XPS software.

2.4. Production of bio-oil *via* fast pyrolysis

Ground to pass a 0.5 mm sieve yellow poplar (*Liriodendron tulipifera*) was used as a raw material for fast pyrolysis. The sample was fed into the reactor with the feeding rate of 1 kg h^{-1}. Fast pyrolysis was accomplished at 500 °C and the residence time was regulated at 1.63 s by inert nitrogen gas flow. The volatile pyrolytic products were cooled and condensed to a liquid bio-oil.

2.5. Hydrodeoxygenation of bio-oil

The prepared catalysts were tested in HDO of bio-oil in a 200 mL stainless steel (SUS316) autoclave reactor. The reactor was equipped with a magnetic stirrer, a thermocouple, a pressure sensor, and a system for controlling the stirring rate,

Open Access Article. Published on 07 March 2017. Downloaded on 1/14/2026 8:37:09 PM.
This article is licensed under a Creative Commons Attribution 3.0 Unported Licence.

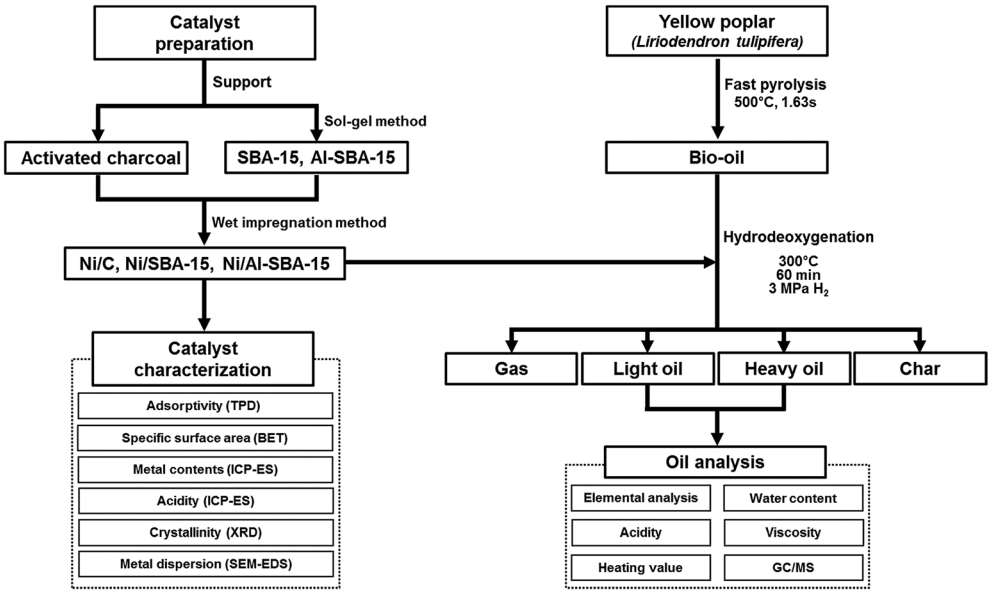

Fig. 1 Scheme of the whole experiment.

temperature and pressure. Before the reaction, the catalysts were activated directly in the reactor by reduction under a H_2 atmosphere at 550 °C for 3 h. After activation, 2 g of the catalysts or supports were added to a mixture of 40 g bio-oil and 10 g ethanol, then placed into the sealed reactor and flushed with N_2. The reactor was then pressurized to 3 MPa H_2, and the temperature was increased to 300 °C.[21,22] After the reaction, there were three phases of products: liquid, char, and gas. The liquid product, consisting of an upper water-rich phase (light oil) and lower organic phase (heavy oil), was recovered from the reactor and separated using a separating funnel. The yields of char, light oil and heavy oil were calculated according to the following equations.

$$\text{- Yield of char (\%)} = [\text{solid (g)} - \text{catalyst (g)}]/[\text{bio-oil (g)} + \text{ethanol (g)}] \times 100$$

$$\text{- Yield of light oil (\%)} = [\text{light oil (g)}]/[\text{bio-oil (g)} + \text{ethanol (g)}] \times 100$$

$$\text{- Yield of heavy oil (\%)} = [\text{heavy oil (g)}]/[\text{bio-oil (g)} + \text{ethanol (g)}] \times 100$$

$$\text{- Yield of gas (\%)} = 100 - [\text{yield of light oil} + \text{yield of heavy oil} + \text{yield of char}]$$

2.6. Characterization of heavy oil

2.6.1. Physicochemical properties. Karl-Fischer titration (TitroLine KF, Schott Instruments, Germany) was used to measure the water content of the bio-oil and heavy oils. In order to investigate the acidity of the bio-oil and heavy oil, the total acid number (TAN) was measured using ASTM D664. The viscosity was determined using a capillary-type viscometer and ViscoClock (Schott Instruments) at 40 °C. Elemental analysis of carbon, hydrogen, and nitrogen was performed out with a LECO CHNS-932 analyzer. The higher heating value (HHV) was calculated using the Sheng and Azevedo's formula.[23] The degree of deoxygenation (DOD) was estimated as follows:

$$\text{Degree of deoxygenation (\%)} = (MO_{\text{bio-oil}} - MO_{\text{heavy oil}})/MO_{\text{bio-oil}} \times 100$$

where $MO_{\text{heavy oil}}$ and $MO_{\text{bio-oil}}$ are the molar oxygen/carbon ratio of heavy oil and bio-oil, respectively.

2.6.2. GC/MS analysis of low molecular compounds. GC/MS analysis with internal standard (I.S; fluoranthene) was performed for qualitative and quantitative analyse of the low-molecular weight compounds in bio-oil and heavy oils. The identification of low-molecular weight compounds in the bio-oil and heavy oil was conducted with an Agilent 7890A coupled with a 5975C mass selective detector (MSD) and a flame ionization detector (FID) equipped with a DB-5 capillary column (60 m × 0.25 mm × 0.25 μm). The oven temperature was maintained at 50 °C for 5 min, followed by heating at a rate of 3 °C min^{-1} to 280 °C and holding for 20 min. The injector and FID detector temperatures were 250 °C and 300 °C, respectively. Fig. 1 describes the overall experimental scheme of this study.

3. Results and discussion

3.1. Synthesis of mesoporous supports and supported nickel catalysts

3.1.1. Physical properties of the supports and Ni catalysts. Table 1 presents the physical properties of the catalysts used in this study. The specific surface areas of Ni/C, Ni7SBA-15, and Ni/Al-SBA-15 were 436.5, 508.7, and 537.7 $m^2 g^{-1}$, while the pores volumes were 0.46, 0.35, and 0.46 $cm^3 g^{-1}$, respectively. These values were lower than those of Pt/C (5 wt%, Sigma-Aldrich), which might be due to the high metal loading (14.6–17.1 wt%). As SBA-15 and Al-SBA-15 were mesoporous-type supports,

 This journal is © The Royal Society of Chemistry 2017

Open Access Article. Published on 07 March 2017. Downloaded on 1/14/2026 8:37:09 PM.
This article is licensed under a Creative Commons Attribution 3.0 Unported Licence.

Table 1 Characterization of synthesized Ni-based catalysts

Sample	Metal content (%)	Si/Al ratio	BET surface area ($m^2\ g^{-1}$)	Micropore area ($m^2\ g^{-1}$)	Pore size (Å)	V_{pore} ($cm^3\ g^{-1}$)	Reduction yield (%)
Active carbon	—	—	896.4	449.8	55.2	0.62	—
SBA-15	—	—	800.2	54.3	55.0	1.08	—
Al-SBA-15	—	2.5	889.2	36.2	32.0	0.73	—
Ni/C	17.1	—	436.5	169.3	59.3	0.43	92.8
Ni/SBA-15	15.4	—	508.7	57.0	44.2	0.65	94.9
Ni/Al-SBA-15	14.6	2.5	537.7	39.1	32.4	0.46	89.5
Pt/C (commercial)	5.0	—	1317.4	243.0	37.6	0.99	—

the micropore areas of Ni/SBA-15 and Ni/Al-SBA-15 (57.0, and 39.1 $m^2\ g^{-1}$, respectively) were lower than that of Ni/C (169.3 $m^2\ g^{-1}$), while the surface area had the opposite tendency. Therefore, Ni/Al-SBA-15, with a high surface area and large pore size, was expected to be effective for good dispersion of the reactant during the reaction.

3.1.2. XRD patterns of the Ni catalysts. Fig. 3 presents the XRD peaks of Ni/C, Ni/SBA-15, and Ni/Al-SBA-15. All samples presented three typical peaks at 2θ 32°, 38° and 58°, marked as (100), (101), and (110), while Ni/C showed more peaks, such as (111) ($2\theta = 47°$). These exhibited that the crystalline properties of SBA-15 and Al-SBA-15 were almost identical. The peaks illustrate that Ni/SBA-15 and Ni/Al-SBA-15 have a hexagonal structure, while Ni/C has a cubic structure.[24–27] Hydroxide ($Ni(OH)_2$) or oxide form (NiO) was investigated in the patterns of Ni/C ($2\theta = 22$, 39°, respectively). It was also found in the XPS results (Section 3.1.3.).

According to the peaks at XRD patterns, Ni particles on Ni/C retained higher dispersion than Ni/SBA-15 or Ni/Al-SBA-15. It was due to the mesoporous structure of SBA-15 and Al-SBA-15, which resulted multi-layered dispersion inside the structure.

3.1.3. Surface binding properties of the catalysts. X-ray photoelectron spectroscopy (XPS) of the catalysts was performed to identify the surface binding properties. Fig. 4 presents the Ni 2p XPS spectra, which exhibit a large band centered at 855.0 eV that can be de-convoluted into two components. The first component at 853 eV was assigned to Ni^0; the low intensity of this band reveals incomplete reduction of nickel.[26] However, the apparent low intensity of this band could be due to the subsequent reabsorption of photoelectrons emerging from the core level of nickel by other nickel atoms of the metallic particles. The peak of the more energetic signal at 856–857 eV reveals either Ni^{2+} ions or very small NiO particles on the walls of the mesopores.[28] These peaks indicated that NiO was partially present, even after the reduction. This band indicated that the reduction is not completely accomplished or should be assigned to the phenomenon that the photoelectrons emerged from the core level of nickel are subsequently reabsorbed by other nickel atoms of the metallic particles. Additionally, the peak at 860 eV is known as the shake-up satellite peak.[29]

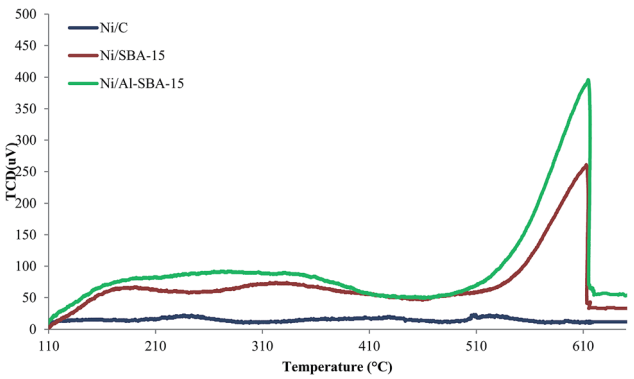

Fig. 2 NH_3-TPD peaks of supports and catalysts.

3.1.4. Surface acidity of the catalysts. The type of surface acidity of the three catalysts was examined by NH_3-TPD measurements (Fig. 2). Since the acid strength of the solid catalyst was defined as its proton-donating ability, the acidity of the synthesized catalyst might have affected the HDO of bio-oil. As shown in Fig. 2, a broad peak near 160–360 °C and a sharp peak at 600 °C were observed for Ni/SBA-15 and Ni/Al-SBA-15, while Ni/C showed no acidic sites. According to previous studies,[30,31] the peaks produced at temperatures above 400 °C are generally attributed to the desorption of NH_3 from strong Brönsted and Lewis sites, while the low-temperature peaks can be attributed (a) desorption of weakly adsorbed NH_3 at weak acid sites or non-acidic sites, (b) weak acid Brönsted and Lewis sites, and (c) formation of $NH^{4+}(NH_3)_n$ groups.[30] During calcination, Ni/SBA-15 and Ni/Al-SBA-15 were quickly increase,[32] and this led to higher strong acid sites and a shift of NH_3-TPD peaks toward higher temperatures.

3.1.5. The morphologies of the supports and Ni catalysts. The morphologies of the supports and catalysts were investigated by SEM (Fig. 5), and SEM-EDS (Fig. 6), respectively. Active charcoal had a rough surface with a spherical shape and small pores (Fig. 5(a)). However, SBA-15 and Al-SBA-15 showed larger structures with smooth surfaces, and round hexagonal prisms. Fig. 6(a)–(c) show that Ni particles in 0.2–0.5 μm were well dispersed within the (a) active charcoal, (b) silica, and (c) alumina–silica matrix. Ni particles were dispersed as multilayers on the SBA-15, and Al-SBA-15 supports, while Ni on the active charcoal was uniformly dispersed on the active charcoal agglomerate, which might be due to the large hexagonal structures of SBA-15 and Al-SBA-15. The impregnation of Ni over the supports led to the formation of Ni/C, Ni/SBA-15 and Ni/Al-SBA-15 catalysts as well as led to the formation of crystalline Ni aggregation on the surface contained partial NiO as evidenced from the phase formation in the high angle XRD.

Open Access Article. Published on 07 March 2017. Downloaded on 1/14/2026 8:37:09 PM.
This article is licensed under a Creative Commons Attribution 3.0 Unported Licence.

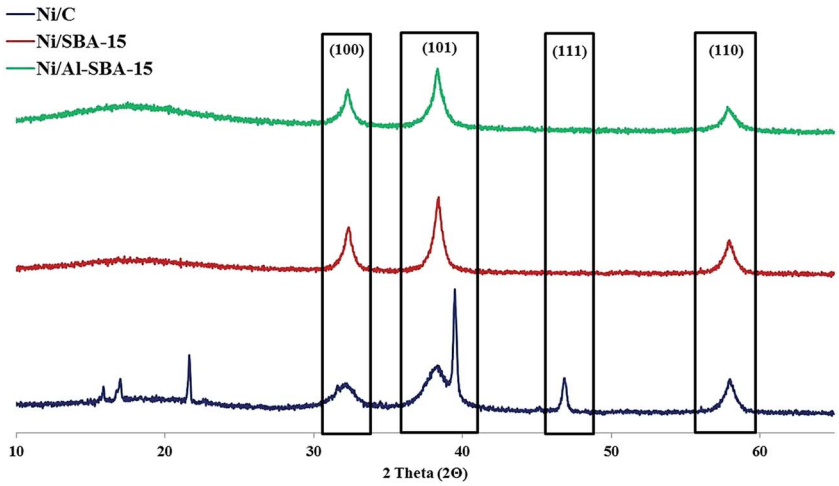

Fig. 3 XRD peaks of supports and catalysts (the peaks of (100), (101), and (110) revealed the hexagonal structure, while (100), (101), (110), and (111) described the cubic structure).

3.2. Catalytic activity

The yields of the HDO products obtained with supports, Ni/C, Ni/SBA-15, and Ni/Al-SBA-15 are shown in Table 2 based on the weight of the bio-oil. The yield of each product revealed that the composition of the HDO products was considerably affected by the support. The products obtained from the HDO with supports showed high yield of tar-like char (71.7–80.4 wt%). The oil phase was not separated into the light and heavy oil. It might be due to the lack of active sites (metal particles) which accelerated the hydrogenation, or deoxygenation. The yield of each product was differed with the type of support. The silica-base supports (SBA-15, and Al-SBA-15) produced less char, more oil and gas phase than active charcoal. The yield of heavy oil showed no significant changes (45.8–48.1%) with Ni-based catalysts. However, the yield was greater than that of Pt/C due to the high metal loading (*ca.* 14–17%) and hexagonal mesoporous structures of the supports. Alternatively, the yields of char, gas, and light oil presented different tendencies with respect to the supports. The active charcoal support produced 9.1% char, 27.1% gas, and 18.0% light oil. When silica-based supports (SBA-15, and Al-SBA-15) were used, 16.8–18.6% char, 6.6–7.1% gas, and 26.7–28.3% light oil were produced. Therefore, active charcoal supports leads to both HDO and further decomposition, while SBA-15 and Al-SBA-15 enhance depolymerization and condensation (charring). The high water content of the light oil might be a result of the dehydration of organic compounds in the oil phase.[33] This might indicate that the structure of the support plays an important role in upgrading bio-oil to heavy oil, as well as producing by-products such as light oil, char, and gas. This process is due to further decomposition of organic compounds in the liquid phase.[34]

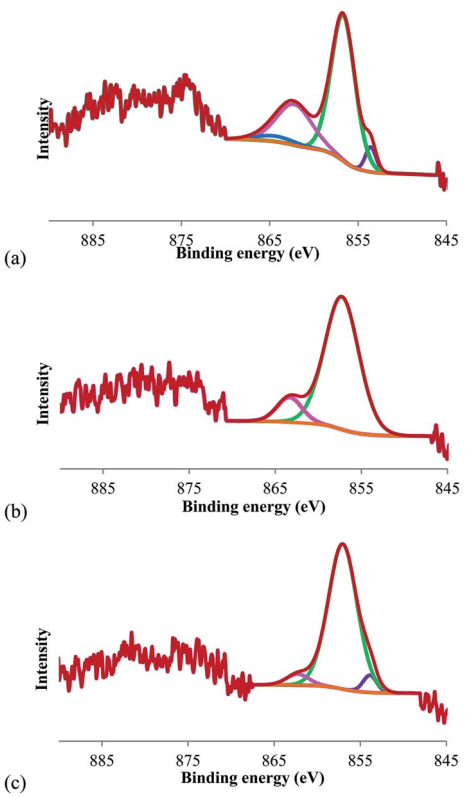

Fig. 4 XPS analysis of Ni 2p spectra on (a) Ni/C, (b) Ni/SBA-15, and (c) Ni/Al-SBA-15 (853 eV: Ni^0; 856–857 eV: Ni^{2+} ions or NiO particles; 860 eV: shake-up satellite peak).

3.3. Fuel properties of heavy oil

3.3.1. Physicochemical features of heavy oil. Typical fuel properties of bio-oil, such as acidity, heating value, and thermal stability, are improved by hydrocracking, hydrogenolysis, dehydration, hydrogenation and deoxygenation during HDO.[34] Therefore, several improved physicochemical properties of heavy oil were measured and are displayed in Table 3. The water content, related to the heating value and combustion properties in the engine, decreased from 17.7% in the bio-oil to 13.0 wt% (Ni/C), 11.4 wt% (Ni/SBA-15), and 9.3 wt% (Ni/Al-SBA-15) in the heavy oils, due to dehydration of the organic phase. Despite the

 This journal is © The Royal Society of Chemistry 2017

Open Access Article. Published on 07 March 2017. Downloaded on 1/14/2026 8:37:09 PM.
This article is licensed under a Creative Commons Attribution 3.0 Unported Licence.

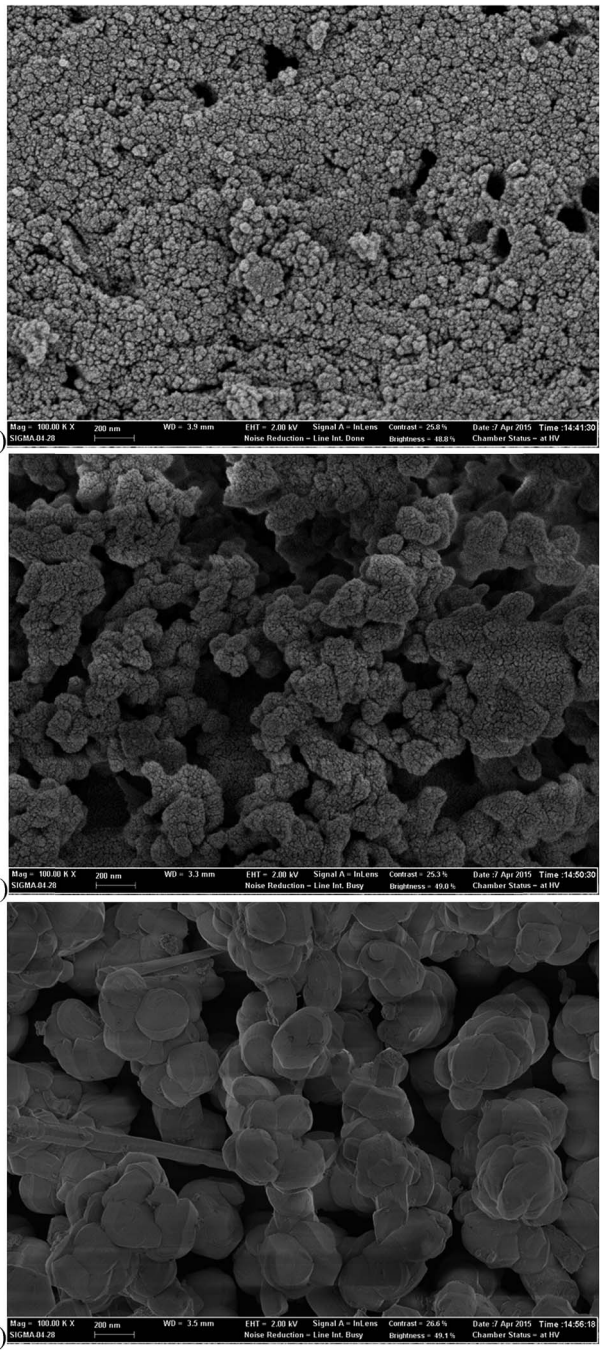

Fig. 5 SEM images of the supports ((a) active charcoal; (b) SBA-15; and (c) Al-SBA-15; scale bar: 200 nm).

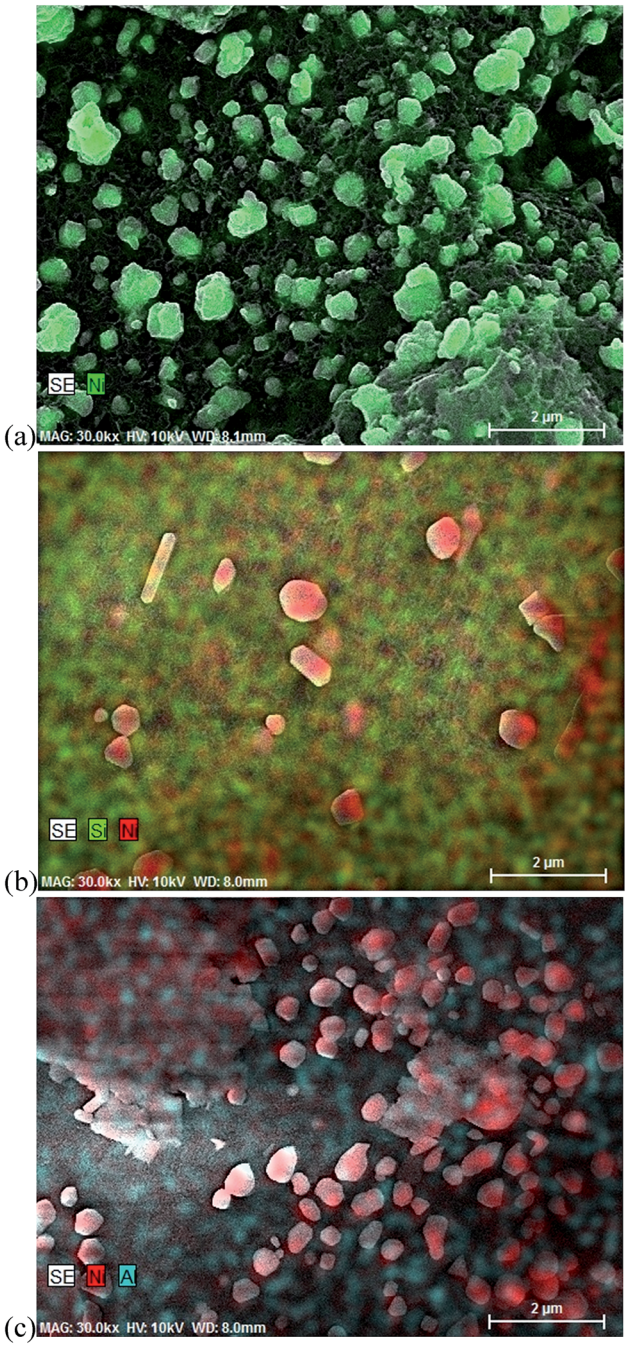

Fig. 6 SEM-EDS images of Ni-based catalysts ((a) Ni/C; (b) Ni/SBA-15; and (c) Ni/Al-SBA-15; scale bar: 2 μm).

high metal loading of Ni/C, the dehydration and de-moisturization capacity were still lower than those of Pt/C. However, the mesoporous hexagonal structure (SBA-15, and Al-SBA-15) effectively catalyzed the de-moisturization, especially the acidic support (Al-SBA-15). Previous study[35] showed that zeolite is effective to dehydration. Since alumina–silica Al-SBA-15 support is consisted of same as zeolite, it is also effective to dehydration.

The TAN of the heavy oil was significantly reduced (50.2–62.2 mg KOH per g oil) in comparison to that of bio-oil (164.8 mg KOH per g oil) and heavy oil obtained from Pt/C (93.2 mg KOH per g oil). Despite acid removal, phenolic compounds should be measured as a weak acid by KOH. Therefore, the acidity level was 50.2–62.2 mg KOH per g in the heavy oils. The compounds derived from carbohydrates, which enhanced the acidity, can be converted into esters and ketones. Moreover, phenolic compounds might also be converted and play an important role in reducing the acidity. Reducing the viscosity is an important point of reforming bio-oil into fuel because the high viscosity of bio-oil results in many

Open Access Article. Published on 07 March 2017. Downloaded on 1/14/2026 8:37:09 PM.
This article is licensed under a Creative Commons Attribution 3.0 Unported Licence.

Table 2 Mass balance of the products obtained from HDO reaction with Ni-catalysts

		Oil phase		
Yield (%)	Char	Light oil	Heavy oil	Gas
Active charcoal	80.4 (0.3)	6.8 (0.0)		12.7 (0.3)
SBA-15	73.8 (0.9)	10.2 (0.3)		16.0 (1.2)
Al/SBA-15	71.7 (0.2)	11.8 (0.2)		16.5 (0.4)
Pt/C[a]	7.7 (0.0)[b]	23.7 (0.4)	35.7 (5.2)	32.8 (2.5)
Ni/C	9.1 (0.7)	18.0 (0.1)	45.8 (2.4)	27.1 (1.4)
Ni/SBA-15	16.8 (0.4)	28.3 (0.5)	47.7 (1.3)	7.1 (0.7)
Ni/Al-SBA-15	18.6 (0.5)	26.7 (0.1)	48.1 (2.0)	6.6 (0.9)

[a] Previous study.[16] [b] Standard deviation.

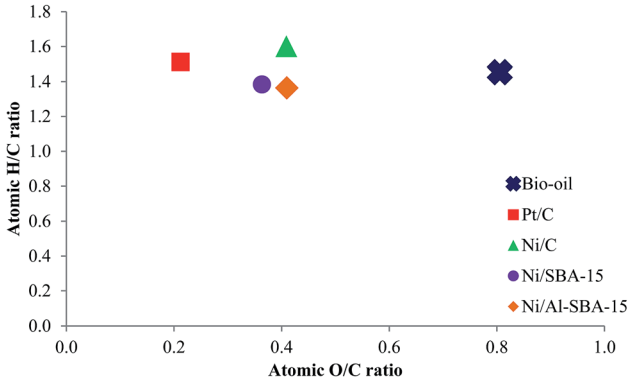

Fig. 7 Van Krevelen diagram of bio-oil, and heavy oils (drybasis).

disadvantages during injection into an engine.[36] In this experiment, the viscosity decreased from 29.6 cSt for bio-oil to 6.8–7.1 cSt for heavy oil. The viscosity is greater than that of the heavy oil obtained from Pt/C, however, the heavy oils also had fluidity and did not stick to the vials.

3.3.2. Elemental composition and calorific value. The elemental compositions of the bio-oil and heavy oil were determined and are presented in Table 3. Compared to the carbon (40.0 wt%), hydrogen (7.5 wt%), and oxygen (52.2 wt%) contents of the bio-oil, the carbon and hydrogen levels increased (54.9–58.9 wt%, and 8.0–9.9 wt%, respectively), while the oxygen level decreased (32.2–34.5 wt%) in heavy oil. The Van Krevelen diagram of the bio-oil, and heavy oils (Fig. 7, dry basis) shows the significant tendency for active charcoal to enhance the hydrogenation, due to the effective dispersion of metal particles on high surface area, and micropore area. Mesoporous silica supports (SBA-15, and Al-SBA-15) exhibited good dehydration due to their acidic sites on the surface. Both supports reduced the atomic O/C ratio from 0.8 (bio-oil) to 0.4 (heavy oils) during the HDO reaction due to the removal of oxygenated compounds in the bio-oil to the gas (Ni/C) or light oil phase (Ni/SBA-15, and Ni/Al-SBA-15) *via* deoxygenation, and the dehydration. Since hydrogenation and deoxygenation was accelerated by the metal sites, the well-dispersed Ni/C (Fig. 3 and 6) is effective to hydrogenation. However, deoxygenation is generally occurred in lignin-derived phenolic compounds, which has large size.[37] Therefore, deoxygenation process might be effectively occurred in mesoporous SBA-15 (Table 1). The reaction also resulted in a greater HHV of the heavy oils (21.9–22.8 MJ kg^{-1}) compared to that of the bio-oil (17.3 MJ kg^{-1}).

3.4. Physicochemical features of light oil

After the HDO reaction, a solvent-based aqueous phase termed light oil was produced as by-product. The physicochemical properties, and organic compounds in the light oil were differed from those of heavy oil. Fig. 8 described representative features of the light oils yielded, such as their water content and acidity. High water content and acidity is remarkable in light oil properties. The water content of the light oil was lower when the Ni-based catalysts were used (43.8–49.7 wt%) than when the Pt/C was used (65.0 wt%). Acidity of light oil presented no significant differences between Pt/C (159.2 mg KOH per g oil), and Ni-based catalysts (160.8–167.4 mg KOH per g oil).

3.5. Degree of deoxygenation (DOD)

Since high oxygen levels result in high acidity, viscosity, and low heating values, deoxygenation is vital to the value-added utilization of bio-oil. HDO leads to decreased oxygen levels in bio-oil through deoxygenation, such as demethoxylation,

Table 3 Physicochemical properties of heavy oil

	Bio-oil[a]	Pt C[a]	Ni/C	Ni/SBA-15	Ni/Al-SBA-15
Water content (wt%)	17.7 (0.2)[e]	0.5 (0.0)	13.0 (0.1)	11.4 (0.2)	9.3 (0.4)
TAN (mg KOH per g oil)	164.8 (0.8)	93.2 (0.5)	50.2 (0.8)	62.2 (1.0)	55.6 (0.1)
Viscosity (cSt)[b]	29.6 (0.2)	4.4 (0.1)	6.8 (0.3)	7.1 (0.0)	6.8 (0.2)
C (wt%)	40.0 (1.0)	70.7 (1.4)	54.9 (1.1)	58.9 (0.7)	57.3 (1.3)
H (wt%)	7.5 (0.2)	9.0 (0.7)	9.9 (1.5)	8.8 (0.6)	8.0 (0.7)
N (wt%)	0.2 (0.0)	0.2 (0.0)	0.7 (0.1)	0.1 (0.0)	0.1 (0.0)
O[c] (wt%)	52.2 (1.4)	20.1 (1.5)	34.4 (0.8)	32.2 (1.4)	34.5 (1.2)
S (wt%)	0.2 (0.0)	0.0 (0.0)	0.0 (0.0)	0.0 (0.0)	0.0 (0.0)
HHV (MJ kg^{-1})[d]	17.3	27.8	21.9	22.8	22.2
Energy efficiency (%)	—	60.3	58.1	62.8	61.7
Degree of deoxygenation	—	73.7	49.2	54.9	49.2

[a] Previous study.[10] [b] Measured at 40 °C. [c] Calculated by difference. [d] High heating value was calculated following formula, drybasis HHV (MJ kg^{-1}) = −1.3675 + (0.3137 × C) + (0.7009 × H) + (0.0318 × O). [e] Standard deviation.

This journal is © The Royal Society of Chemistry 2017

Open Access Article. Published on 07 March 2017. Downloaded on 1/14/2026 8:37:09 PM.
This article is licensed under a Creative Commons Attribution 3.0 Unported Licence.

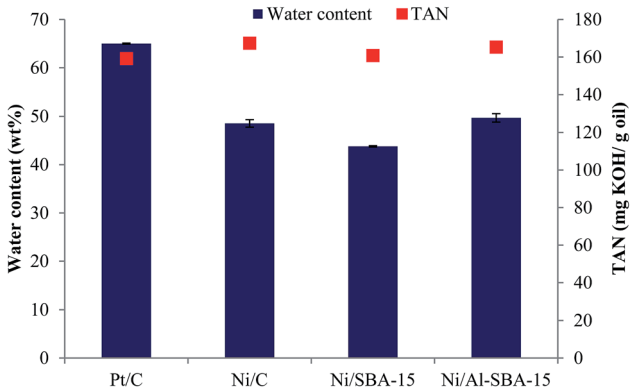

Fig. 8 Physicochemical properties of light oil.

dehydroxylation, or dehydration. The DOD was calculated based on the atomic O/C ratio. After the HDO, the O/C ratio of the bio-oil (0.8) decreased to *ca.* 0.4 due to deoxygenation. There were no significant differences among the various supports. The DOD varied between 49.2 and 54.9% with Ni-based catalysts. Ni/SBA-15 showed the highest DOD level (54.9%), which suggests the high pore volume of the catalyst (0.65 $cm^3\ g^{-1}$), and large pore size (44.2 Å) reacted with the oxygenated compounds.[34] The decrease in H/C ratio in the heavy oil obtained from Ni/SBA-15 and Ni/Al-SBA-15 (1.4) compared to that of bio-oil (1.5) could have resulted from dehydration and deoxygenation. In conclusion, dehydration can occur on both Ni particles and mesoporous silica supports (SBA-15 and Al-SBA-15), while active charcoal enables metal dispersion.[38]

3.6. Structural modification of low-molecular weight compounds during HDO

Twenty-two typical compounds in bio-oil, heavy oil, and light oil were identified from the GC/MS analysis and classified based on chemical structure and functional groups. Their relative amounts are presented in Tables 4 and 5 (heavy oil and light oil, respectively). The Ni-based catalysts mainly generated compounds in heavy oil categorized as guaiacols, such as guaiacol, 4-ethyl-guaiacol, and 4-propyl-guaiacol. The minor compounds, such as esters, ketones, and other phenolic compounds, were also present in heavy oil after the HDO. The heavy oils showed a 65.7–76.4% decrease in the total compounds compared to bio-oil. The decrease typically resulted from decarboxylation and further decomposition of acetic acid, furfural, vanillin, and levoglucosan or separation into the light oil phase. Significantly, the light oil phase consisted mostly of acetic acid and acetic acid ethyl ester (Table 5).

Generation of catechol and *p*-cresol and removal of 4-ethyl-phenol and 3,4-dihydroxyacetophenone suggest that Ni-based catalyst can accelerate dealkylation or transalkylation. However, the remaining 4-propyl-guaiacol and producion of 4-propyl-syringol suggest that Ni-based catalysts might not effectively reduce the activation energy of dealkylation, or decomposition. Additionally, less CH_4 was observed than in Pt/C (Table 6). Guaiacol and syringol remained abundant in the heavy oil, despite demethoxylation to phenol. This result was due to the dealkylation, or demethoxylation *via* hydrogenation[34] and was confirmed by the elimination of 4-methyl-syringol and 4-(1-propenyl)-guaiacol. The unstable and undesired acetic acid,

Table 4 Quantitative analysis of major micromolecular components in the bio-oil and heavy oils by GC/MS analysis

			Amount (mg mL^{-1} bio-oil)				
	No.	Compound	Bio-oil	Pt/C	Ni/C	Ni/SBA-15	Ni/Al-SBA-15
Acids	1	Acetic acid	28.0	8.2	—	—	—
Esters	2	Acetic acid, ethyl ester	—	14.6	24.5	28.1	7.7
Ketones	3	Cyclopentanone	—	2.0	0.9	1.8	3.3
	4	2-Methyl-cyclopentanone	—	0.7	—	—	—
Phenols	5	Phenol	—	9.5	0.5	0.3	0.5
	6	*p*-Cresol	—	3.4	1.8	2.3	1.3
	7	Guaiacol	3.3	16.7	11.9	12.2	11.9
	8	4-Ethyl-phenol	0.4	—	—	—	—
	9	Creosol	1.1	3.0	—	1.9	10.0
	10	4-Vinyl-phenol	0.4	—	—	—	—
	11	2-Propyl-phenol	1.2	—	—	—	—
	12	Catechol	—	1.6	3.1	1.6	1.4
	13	4-Ethyl-guaiacol	1.1	6.6	4.0	5.8	5.5
	14	3,4-Dihydroxyacetophenone	0.7	—	—	—	—
	15	Syringol	0.4	7.7	1.6	1.4	2.6
	16	4-Propyl-guaiacol	2.1	7.1	3.9	5.6	3.5
	17	4-Methyl-syringol	0.5	—	—	—	—
	18	4-(1-Propenyl)-guaiacol	0.7	—	—	—	—
	19	4-Propyl-syringol	—	9.1	4.1	7.2	3.6
Sum of Phenols			11.9	64.7	30.9	38.3	40.3
Aldehydes	20	Furfural	7.6	—	—	—	—
	21	Vanillin	1.2	—	—	—	—
Sugars	22	Levoglucosan	27.0	—	—	—	—
Total			75.7	90.2	56.3	68.2	51.3

Open Access Article. Published on 07 March 2017. Downloaded on 1/14/2026 8:37:09 PM.
This article is licensed under a Creative Commons Attribution 3.0 Unported Licence.

Table 5 Quantitative analysis of major micromolecular components in the bio-oil and light oils by GC/MS analysis

			Amount (mg mL^{-1} bio-oil)				
	No.	Compound	Bio-oil	Pt/C	Ni/C	Ni/SBA-15	Ni/Al-SBA-15
Acids	1	Acetic acid	28.0	58.3	93.3	107.3	133.0
Esters	2	Acetic acid, ethyl ester	—	5.5	75.1	91.7	82.4
Ketones	3	Cyclopentanone	—	0.2	1.8	4.4	5.5
	4	2-Methyl-cyclopentanone	—	3.5	—	—	—
Phenols	5	Phenol	—	0.4	—	—	—
	6	*p*-Cresol	—	3.0	0.8	2.2	0.8
	7	Guaiacol	3.3	7.1	5.9	7.8	7.1
	8	4-Ethyl-phenol	0.4	—	—	—	—
	9	Creosol	1.1	—	7.1	—	—
	10	4-Vinyl-phenol	0.4	—	—	—	—
	11	2-Propyl-phenol	1.2	—	—	—	—
	12	Catechol	—	9.1	2.9	3.3	2.9
	13	4-Ethyl-guaiacol	1.1		1.8	2.6	2.6
	14	3,4-Dihydroxyacetophenone	0.7	—	—	—	—
	15	Syringol	0.4	3.7	5.1	1.4	1.0
	16	4-Propyl-guaiacol	2.1	—	—	—	2.5
	17	4-Methyl-syringol	0.5	—	—	—	—
	18	4-(1-Propenyl)-guaiacol	0.7	—	—	—	—
	19	4-Propyl-syringol	—	—	—	3.6	1.8
Sum of Phenols			11.9	23.3	23.6	20.9	18.7
Aldehydes	20	Furfural	7.6	—	—	—	—
	21	Vanillin	1.2	—	—	—	—
Sugars	22	Levoglucosan	27.0	—	—	—	—
Total			75.7	90.8	193.8	224.3	239.6

Table 6 Distribution of representative gas components determined by TCD-FID after HDO reaction

Concentration (%)	Active charcoal	SBA-15	Al/SBA-15	Pt/C	Ni/C	Ni/SBA-15	Ni/Al-SBA-15
CH_4	16.7 (2.3)	12.4 (1.7)	13.6 (1.3)	24.1 (1.0)	7.1 (0.0)	2.3 (0.0)	5.8 (0.0)
CO	70.6 (1.4)	63.3 (2.1)	77.9 (1.8)	70.9 (1.4)	88.4 (0.7)	94.9 (1.8)	90.1 (1.5)
C_2H_4	6.5 (0.0)	19.6 (0.3)	3.2 (0.0)	0.3 (0.0)	—	—	—
C_2H_2	2.5 (0.0)	1.9 (0.0)	1.8 (0.0)	—	1.5 (0.3)	0.6 (0.0)	1.5 (0.1)
C_3H_6	—	—	—	3.2 (0.0)	—	—	—
C_3H_8	3.7 (0.4)	2.8 (0.0)	3.6 (0.1)	1.6 (0.0)	3.1 (0.0)	2.2 (0.0)	2.7 (0.0)

furfural and levoglucosan in the bio-oil were totally converted to acetic acid ethyl esters, and cyclopentanone in the heavy oil *via* hydrogenation, decarbonylation, dehydroxylation, and ring opening, or low molecular gas phase. Additionally, heavy oil obtained from Ni/Al-SBA-15 yielded low levels of acetic acid ethyl ester, and a high level of cyclopentanone. Therefore, Ni/Al-SBA-15 might be the most effective support to convert unstable carbohydrate derivatives into a stable form.[36]

3.7. Gas composition

Gas phase analysis was performed, and the distribution is shown in Table 6. The results revealed the formation of CH_4, CO, C_2H_2, and C_3H_8 when HDO was performed with Ni-based catalysts, and supports. Compared with Ni-based catalysts, the gas phase obtained from HDO with supports contained more hydrocarbon gas. For effective hydrogenation, and deoxygenation, the metal active sites are essential. The CH_4 yield was lower with Ni-based catalysts compared to that with Pt/C. HDO with Ni/SBA-15 produced 2.3% CH_4, while Ni/Al-SBA-15 and Ni/C produced 5.8 and 7.1%, respectively. However, CO concentrations increased significantly when solvent Ni-based catalysts were used, especially Ni/SBA-15 (94.9%), possibly due to release through decarboxylation.[39] The observed 2.3–7.1% of CH_4 generally originated from demethylation and slight hydrogenation.[34] The highest CH_4 concentration (7.1%) was observed when active charcoal was used as a support, whereas the use of mesoporous silica supports allowed the release of a larger amount of CO. The non-acidic SBA-15 support especially allowed hydrogenation, and inhibited dealkylation according to the low concentrations of CH_4, C_2H_2, and C_3H_8 that likely originated from dealkylation of phenolic side chains.

4. Conclusions

Mesoporous SBA-15, and Al-SBA-15 were synthesized *via* the sol–gel method, and Ni-based catalysts (Ni/C, Ni/SBA-15, and

 This journal is © The Royal Society of Chemistry 2017

Open Access Article. Published on 07 March 2017. Downloaded on 1/14/2026 8:37:09 PM.
This article is licensed under a Creative Commons Attribution 3.0 Unported Licence.

Ni/Al-SBA-15) were prepared by a wet impregnation method. The characterization of the catalysts showed that Al-SBA-15 had a highly-ordered hexagonal structure, and Ni particles were well dispersed on the supports. The catalytic properties of the bio-oil HDO were investigated in an autoclave reactor. HDO was affected by the catalyst supports, and bio-oil was converted to gas, char, light oil, and heavy oil. The results of the HDO indicated that mesoporous silica supports (SBA-15, and Al-SBA-15) exhibited greater activity than Ni supported on active charcoal (Ni/C). The higher activity of the catalyst could be correlated to its high surface area, and pore size, which uniformly dispersed the Ni particles. The physicochemical properties of bio-oil, such as water content, viscosity, acidity, oxygen level, and HHV, improved after HDO, with differences in catalyst support type. Based on the results, hydrogenation (active charcoal), deoxygenation (SBA-15), and dehydration (Al-SBA-15) can be effectively enhanced during the reaction and affect heavy oil properties.

Acknowledgements

This research was supported by Research Resettlement Fund for the new faculty of Seoul National University and funded by the Korea Institute of Planning and Evaluation for Technology in Food, Agriculture, Forestry and Fisheries (IPET) through Agri-Bio Industry Technology Development Program, funded by Ministry of Agriculture, Food and Rural Affairs (MAFRA) (No. 115092021CG000).

References

1 E. Furimsky, Catalytic hydrodeoxygenation, *Appl. Catal., A*, 2000, **199**, 147–190.
2 P. S. Rezaei, H. Shafaghat and W. M. A. W. Daud, Production of green aromatics and olefins by catalytic cracking of oxygenate compounds derived from biomass pyrolysis: A review, *Appl. Catal., A*, 2014, **469**, 490–511.
3 L. Zhang, R. Liu, R. Yin and Y. Mei, Upgrading of bio-oil from biomass fast pyrolysis in China: A review, *Renewable Sustainable Energy Rev.*, 2013, **24**, 66–72.
4 T. Choudhary and C. Phillips, Renewable fuels *via* catalytic hydrodeoxygenation, *Appl. Catal., A*, 2011, **397**, 1–12.
5 M. Á. González-Borja and D. E. Resasco, Anisole and guaiacol hydrodeoxygenation over monolithic Pt–Sn catalysts, *Energy Fuels*, 2011, **25**, 4155–4162.
6 X. Zhu, L. L. Lobban, R. G. Mallinson and D. E. Resasco, Bifunctional transalkylation and hydrodeoxygenation of anisole over a Pt/HBeta catalyst, *J. Catal.*, 2011, **281**, 21–29.
7 A. L. Jongerius, R. Jastrzebski, P. C. Bruijnincx and B. M. Weckhuysen, CoMo sulfide-catalyzed hydrodeoxygenation of lignin model compounds: An extended reaction network for the conversion of monomeric and dimeric substrates, *J. Catal.*, 2012, **285**, 315–323.
8 A. Narani, R. K. Chowdari, C. Cannilla, G. Bonura, F. Frusteri, H. J. Heeres and K. Barta, Efficient catalytic hydrotreatment of Kraft lignin to alkylphenolics using supported NiW and NiMo catalysts in supercritical methanol, *Green Chem.*, 2015, **17**, 5046–5057.
9 N. Yan, Y. Yuan, R. Dykeman, Y. Kou and P. J. Dyson, Hydrodeoxygenation of Lignin-Derived Phenols into Alkanes by Using Nanoparticle Catalysts Combined with Brønsted Acidic Ionic Liquids, *Angew. Chem., Int. Ed.*, 2010, **49**, 5549–5553.
10 Y. Wang, S. De and N. Yan, Rational control of nano-scale metal-catalysts for biomass conversion, *Chem. Commun.*, 2016, **52**, 6210–6224.
11 S. De, J. Zhang, R. Luque and N. Yan, Ni-based bimetallic heterogeneous catalysts for energy and environmental applications, *Energy Environ. Sci.*, 2016, **9**, 3314–3347.
12 T. M. Huynh, U. Armbruster, M. M. Pohl, M. Schneider, J. Radnik, D. L. Hoang, B. M. Q. Phan, D. A. Nguyen and A. Martin, Hydrodeoxygenation of Phenol as a Model Compound for Bio-oil on Non-noble Bimetallic Nickel-based Catalysts, *ChemCatChem*, 2014, **6**, 1940–1951.
13 X. Wang and R. Rinaldi, Solvent effects on the hydrogenolysis of diphenyl ether with Raney nickel and their implications for the conversion of lignin, *ChemSusChem*, 2012, **5**, 1455–1466.
14 J. Zhang, J. Teo, X. Chen, H. Asakura, T. Tanaka, K. Teramura and N. Yan, A series of NiM (M = Ru, Rh, and Pd) bimetallic catalysts for effective lignin hydrogenolysis in water, *ACS Catal.*, 2014, **4**, 1574–1583.
15 I. T. Ghampson, C. Sepúlveda, R. Garcia, J. G. Fierro, N. Escalona and W. J. DeSisto, Comparison of alumina- and SBA-15-supported molybdenum nitride catalysts for hydrodeoxygenation of guaiacol, *Appl. Catal., A*, 2012, **435**, 51–60.
16 Q. Lu, Z. Tang, Y. Zhang and X.-f. Zhu, Catalytic upgrading of biomass fast pyrolysis vapors with Pd/SBA-15 catalysts, *Ind. Eng. Chem. Res.*, 2010, **49**, 2573–2580.
17 S. Lestari, P. Mäki-Arvela, K. Eränen, J. Beltramini, G. M. Lu and D. Y. Murzin, Diesel-like hydrocarbons from catalytic deoxygenation of stearic acid over supported Pd nanoparticles on SBA-15 catalysts, *Catal. Lett.*, 2010, **134**, 250–257.
18 D. Zhao, J. Feng, Q. Huo, N. Melosh, G. H. Fredrickson, B. F. Chmelka and G. D. Stucky, Triblock copolymer syntheses of mesoporous silica with periodic 50 to 300 angstrom pores, *Science*, 1998, **279**, 548–552.
19 V. Mohan, C. Pramod, M. Suresh, K. H. P. Reddy, B. D. Raju and K. R. Rao, Advantage of Ni/SBA-15 catalyst over Ni/MgO catalyst in terms of catalyst stability due to release of water during nitrobenzene hydrogenation to aniline, *Catal. Commun.*, 2012, **18**, 89–92.
20 A. Galarneau, H. Cambon, F. Di Renzo, R. Ryoo, M. Choi and F. Fajula, Microporosity and connections between pores in SBA-15 mesostructured silicas as a function of the temperature of synthesis, *New J. Chem.*, 2003, **27**, 73–79.
21 S. Oh, H. Hwang, H. S. Choi and J. W. Choi, Investigation of chemical modifications of micro-and macromolecules in bio-oil during hydrodeoxygenation with Pd/C catalyst in supercritical ethanol, *Chemosphere*, 2014, **117**, 806–814.

Open Access Article. Published on 07 March 2017. Downloaded on 1/14/2026 8:37:09 PM.
This article is licensed under a Creative Commons Attribution 3.0 Unported Licence.

22 S. Oh, H. Hwang, H. S. Choi and J. W. Choi, The effects of noble metal catalysts on the bio-oil quality during the hydrodeoxygenative upgrading process, *Fuel*, 2015, **153**, 535–543.

23 C. Sheng and J. Azevedo, Estimating the higher heating value of biomass fuels from basic analysis data, *Biomass Bioenergy*, 2005, **28**, 499–507.

24 N. Wang, X. Yu, k. Shen, W. Chu and W. Qian, Synthesis, characterization and catalytic performance of MgO-coated Ni/SBA-15 catalysts for methane dry reforming to syngas and hydrogen, *Int. J. Hydrogen Energy*, 2013, **38**, 9718–9731.

25 W. Zhang, D. Yu, X. Ji and H. Huang, Efficient dehydration of bio-based 2,3-butanediol to butanone over boric acid modified HZSM-5 zeolites, *Green Chem.*, 2012, **14**, 3441–3450.

26 W. Yu, Y. Tang, L. Mo, P. Chen, H. Lou and X. Zheng, Bifunctional Pd/Al-SBA-15 catalyzed one-step hydrogenation–esterification of furfural and acetic acid: a model reaction for catalytic upgrading of bio-oil, *Catal. Commun.*, 2011, **13**, 35–39.

27 M. Kruk, M. Jaroniec, C. H. Ko and R. Ryoo, Characterization of the porous structure of SBA-15, *Chem. Mater.*, 2000, **12**, 1961–1968.

28 F. de Miguel Mercader, M. J. Groeneveld, S. R. Kersten, C. Geantet, G. Toussaint, N. W. Way, C. J. Schaverien and K. J. Hogendoorn, Hydrodeoxygenation of pyrolysis oil fractions: process understanding and quality assessment through co-processing in refinery units, *Energy Environ. Sci.*, 2011, **4**, 985–997.

29 N. Joshi and A. Lawal, Hydrodeoxygenation of pyrolysis oil in a microreactor, *Chem. Eng. Sci.*, 2012, **74**, 1–8.

30 R. Martínez-Palou, M. L. Mosqueira, B. Zapata-Rendón, E. Mar-Juárez, C. Bernal-Huicochea, J. de la Cruz Clavel-López and J. Aburto, Transportation of heavy and extra-heavy crude oil by pipeline: A review, *J. Pet. Sci. Eng.*, 2011, **75**, 274–282.

31 Y. Yu, X. Li, L. Su, Y. Zhang, Y. Wang and H. Zhang, The role of shape selectivity in catalytic fast pyrolysis of lignin with zeolite catalysts, *Appl. Catal., A*, 2012, **447**, 115–123.

32 Y. Aponte and H. I. de Lasa, The Effect of Zn on Offretite Zeolite Properties. Acidic Characterizations and NH_3-TPD Desorption Models, *Ind. Eng. Chem. Res.*, 2017, **56**, 1948–1960.

33 C. Zhao, Y. Kou, A. A. Lemonidou, X. Li and J. A. Lercher, Highly Selective Catalytic Conversion of Phenolic Bio-Oil to Alkanes, *Angew. Chem.*, 2009, **121**, 4047–4050.

34 E. Furimsky, J. Mikhlin, D. Jones, T. Adley and H. Baikowitz, On the mechanism of hydrodeoxygenation of ortho substituted phenols, *Can. J. Chem. Eng.*, 1986, **64**, 982–985.

35 M. Shemfe, S. Gu and B. Fidalgo, Techno-economic analysis of biofuel production *via* bio-oil zeolite upgrading: An evaluation of two catalyst regeneration systems, *Biomass Bioenergy*, 2017, **98**, 182–193.

36 C. Ochoa-Hernández, Y. Yang, P. Pizarro, A. Víctor, J. M. Coronado and D. P. Serrano, Hydrocarbons production through hydrotreating of methyl esters over Ni and Co supported on SBA-15 and Al-SBA-15, *Catal. Today*, 2013, **210**, 81–88.

37 Y. Yu, X. Li, L. Su, Y. Zhang, Y. Wang and H. Zhang, The role of shape selectivity in catalytic fast pyrolysis of lignin with zeolite catalysts, *Appl. Catal., A*, 2012, **447**, 115–123.

38 S.-K. Wu, P.-C. Lai and Y.-C. Lin, Atmospheric Hydrodeoxygenation of Guaiacol over Nickel Phosphide Catalysts: Effect of Phosphorus Composition, *Catal. Lett.*, 2014, **144**, 878–889.

39 O. Şenol, T.-R. Viljava and A. Krause, Hydrodeoxygenation of methyl esters on sulphided NiMo/γ-Al_2O_3 and CoMo/γ-Al_2O_3 catalysts, *Catal. Today*, 2005, **100**, 331–335.

 This journal is © The Royal Society of Chemistry 2017